# COSMIC RAYS

To reduce the size of this section's PostScript file, we have divided it into two PostScript files. We present the following index:

PART 1


| Page # | Section name | |
|---|---|---|
| 1 | 20.1 | Primary spectra |
| 2 | 20.2 | Cosmic rays in the atmosphere |
| 5 | 20.3 | Cosmic rays at the surface |


PART 2


| Page # | Section name | |
|---|---|---|
| 8 | 20.4 | Cosmic rays underground |
| 11 | 20.5 | Air showers |
| 14 | | References |

## 20.4. Cosmic rays underground

Only muons and neutrinos penetrate to significant depths underground. The muons produce tertiary fluxes of photons, electrons, and hadrons.

**20.4.1.** ***Muons***: As discussed in Section 23.6 of this *Review*, muons lose energy by ionization and by radiative processes: bremsstrahlung, direct production of $e^+e^-$ pairs, and photonuclear interactions. The total muon energy loss may be expressed as a function of the amount of matter traversed as

$$-\frac{dE_\mu}{dX} = a + b\,E_\mu \ , \tag{20.6}$$

where $a$ is the ionization loss and $b$ is the fractional energy loss by the three radiation processes. Both are slowly varying functions of energy. The quantity $\epsilon \equiv a/b$ ($\approx 500$ GeV in standard rock) defines a critical energy below which continuous ionization loss is more important the radiative losses. Table 20.2 shows $a$ and $b$ values for standard rock as a function of muon energy. The second column of Table 20.2 shows the muon range in standard rock ($A = 22$, $Z = 11$, $\rho = 2.65$ g cm$^{-3}$). These parameters are quite sensitive to the chemical composition of the rock, which must be evaluated for each experimental location.

**Table 20.2:** Average muon range $R$ and energy loss parameters calculated for standard rock. Range is given in km-water-equivalent, or $10^5$ g cm$^{-2}$.

| $E_\mu$ | R | $a$ | $b_{\rm pair}$ | $b_{\rm brems}$ | $b_{\rm nucl}$ | $\sum b_i$ |
|---|---|---|---|---|---|---|
| GeV | km.w.e. | MeV g$^{-1}$ cm$^2$ | ——— | $10^{-6}$ g$^{-1}$ cm$^2$ | | ——— |
| 10 | 0.05 | 2.15 | 0.73 | 0.74 | 0.45 | 1.91 |
| 100 | 0.41 | 2.40 | 1.15 | 1.56 | 0.41 | 3.12 |
| 1000 | 2.42 | 2.58 | 1.47 | 2.10 | 0.44 | 4.01 |
| 10000 | 6.30 | 2.76 | 1.64 | 2.27 | 0.50 | 4.40 |

The intensity of muons underground can be estimated from the muon intensity in the atmosphere and their rate of energy loss. To the extent that the mild energy dependence of $a$ and $b$ can be neglected, Eq. (20.6) can be integrated to provide the following relation between the energy $E_{\mu,0}$ of a muon at production in the atmosphere and its average energy $E_\mu$ after traversing a thickness $X$ of rock (or ice or water):

$$E_\mu = (E_{\mu,0} + \epsilon)\,e^{-bX} - \epsilon \ . \tag{20.7}$$

Especially at high energy, however, fluctuations are important and an accurate calculation requires a simulation that accounts for stochastic energy-loss processes [21].

Fig. 20.5 shows the vertical muon intensity versus depth. In constructing this "depth-intensity curve," each group has taken account of the angular distribution of the

muons in the atmosphere, the map of the overburden at each detector, and the properties of the local medium in connecting measurements at various slant depths and zenith angles to the vertical intensity. Use of data from a range of angles allows a fixed detector to cover a wide range of depths. The flat portion of the curve is due to muons produced locally by charged-current interactions of $\nu_\mu$.

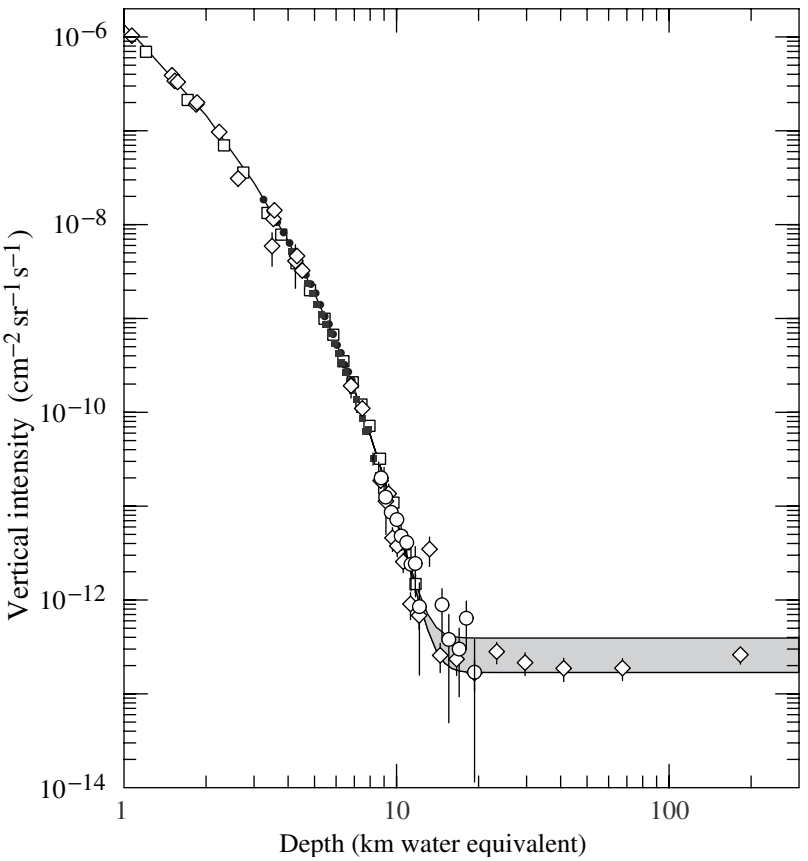


**Figure 20.5:** Vertical muon intensity *vs.* depth (1 km.w.e.= $10^5$ g cm$^{-2}$ of standard rock). The experimental data are from: ◊: the compilations of Crouch [29], □: Baksan [30], ○ : LVD [31], ● : MACRO [32], ■: Frejus [33]. The shaded area at large depths represents neutrino induced muons of energy above 2 GeV. The upper line is for horizontal neutrino-induced muons, the lower one for vertically upward muons.

The energy spectrum of atmospheric muons underground can be estimated from Eq. (20.7). The muon energy spectrum at slant depth $X$ is

$$\frac{dN_\mu(X)}{dE_\mu} = \frac{dN_\mu}{dE_{\mu,0}}\, e^{bX} \ , \tag{20.8}$$

where $E_{\mu,0}$ is the solution of Eq. (20.7). For $X \ll b^{-1} \approx 2.5$ km water equivalent, $E_{\mu,0} \approx E_\mu(X) + aX$. Thus at shallow depths the differential muon energy spectrum is approximately constant for $E_\mu < aX$ and steepens to reflect the surface muon spectrum for $E_\mu > aX$. For $X \gg b^{-1}$ the differential spectrum underground is again constant for small muon energies but steepens to reflect the surface muon spectrum for $E_\mu > \epsilon \approx 0.5$ TeV. In this regime the shape is independent of depth although the intensity decreases exponentially with depth.

**20.4.2.** ***Neutrinos***: Because neutrinos have small interaction cross sections, measurements of atmospheric neutrinos require a deep detector to avoid backgrounds. There are two types of measurements: contained (or semi-contained) events, in which the vertex is determined to originate inside the detector, and neutrino-induced muons. The latter are muons that enter the detector from zenith angles so large (*e.g.*, nearly horizontal or upward) that they cannot be muons produced in the atmosphere. In neither case is the neutrino flux measured directly. What is measured is a convolution of the neutrino flux and cross section with the properties of the detector (which includes the surrounding medium in the case of entering muons).

Contained events reflect the neutrinos in the GeV region where the product of increasing cross section and decreasing flux is maximum. In this energy region the neutrino flux and its angular distribution depend on the geomagnetic location of the detector and to a lesser extent on the phase of the solar cycle. Naively, we expect $\nu_\mu/\nu_e = 2$ from counting the neutrinos of the two flavors coming from the chain of pion and muon decay. This ratio is only slightly modified by the details of the decay kinematics. Experimental measurements have also to account for the ratio of $\overline{\nu}/\nu$, which have cross sections different by a factor of 3 in this energy range. In addition, detectors will generally have different efficiencies for detecting muon neutrinos and electron neutrinos. Even after correcting for these and other effects, some detectors [22,23] infer a $\nu_\mu/\nu_e$ ratio lower by $\approx 4\sigma$ from the expected value. (See Tables in the Particle Listings of this *Review.*) This effect is sometimes cited as possible evidence of neutrino oscillations and is a subject of current investigation. Figure 20.6 shows the data of Refs. 22,23 for the distributions of visible energy in electron-like and muon-like charged-current events, which appear to be nearly equal in number. Corrections for detection efficiencies and backgrounds are insufficient to account for the difference from the expected value of two.

Muons that enter the detector from outside after production in charged-current interactions of neutrinos naturally reflect a higher energy portion of the neutrino spectrum than contained events because the muon range increases with energy as well as the cross section. The relevant energy range is $\sim 10 < E_\nu < 1000$ GeV, depending somewhat on angle. Like muons (see Eq. (20.5)), high energy neutrinos show a "secant theta" effect which causes the flux of horizontal neutrino induced muons to be approximately a factor two higher than the vertically upward flux. The upper and lower edges of the horizontal shaded region in Fig. 20.5 correspond to horizontal and vertical intensities of neutrino-induced muons. Table 20.3 gives the measured fluxes of neutrino induced muons.

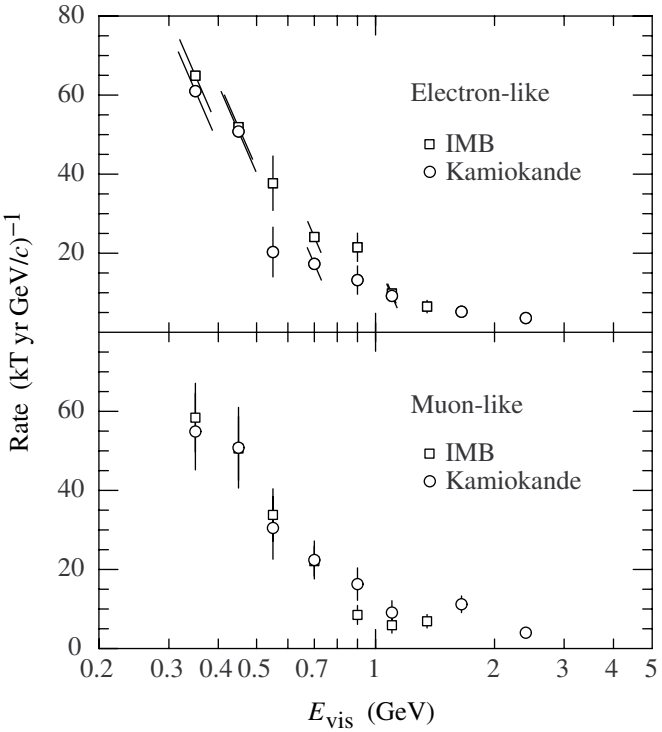


**Figure 20.6:** Contained neutrino interactions from IMB [23](□) and Kamiokande [22].

**Table 20.3:** Measured fluxes ($10^{-13}$ cm$^{-2}$ s$^{-1}$ sr$^{-1}$) of neutrino-induced muons as a function of the minimum muon energy $E_\mu$.

| $E_\mu >$ | 1 GeV | 1 GeV | 1 GeV | 2 GeV | 3 GeV |
|---|---|---|---|---|---|
| Ref. | CWI [24] | Baksan [25] | MACRO [26] | IMB [27] | Kam [28] |
| $F_\mu$ | 2.17±0.21 | 2.77±0.17 | 2.48 ± 0.27 | 2.26±0.11 | 2.04±0.13 |

## 20.5. Air showers

So far we have discussed inclusive or uncorrelated fluxes of various components of the cosmic radiation. An air shower is caused by a single cosmic ray with energy high enough for its cascade to be detectable at the ground. The shower has a hadronic core, which acts as a collimated source of electromagnetic subshowers, generated mostly from $\pi^0 \to \gamma\gamma$. The resulting electrons and positrons are the most numerous particles in the shower. The number of muons, produced by decays of charged mesons, is an order of magnitude lower.

Air showers spread over a large area on the ground, and arrays of detectors operated for long times are useful for studying cosmic rays with primary energy $E_0 > 100$ TeV,

where the low flux makes measurements with small detectors in balloons and satellites difficult.

Greisen [46] gives the following approximate expressions for the numbers and lateral distributions of particles in showers at ground level. The total number of muons $N_\mu$ with energies above 1 GeV is

$$N_\mu(> 1 \text{ GeV}) \approx 0.95 \times 10^5 \left(\frac{N_e}{10^6}\right)^{3/4} , \tag{20.9}$$

where $N_e$ is the total number of charged particles in the shower (not just $e^\pm$). The number of muons per square meter, $\rho_\mu$, as a function of the lateral distance $r$ (in meters) from the center of the shower is

$$\rho_\mu = \frac{1.25\, N_\mu}{2\pi\, \Gamma(1.25)} \left(\frac{1}{320}\right)^{1.25} r^{-0.75} \left(1 + \frac{r}{320}\right)^{-2.5} , \tag{20.10}$$

where $\Gamma$ is the gamma function. The number density of charged particles is

$$\rho_e = C_1(s, d, C_2)\, x^{(s-2)}(1 + x)^{(s-4.5)}(1 + C_2 x^d) . \tag{20.11}$$

Here $s$, $d$, and $C_2$ are parameters in terms of which the overall normalization constant $C_1(s, d, C_2)$ is given by

$$C_1(s, d, C_2) = \frac{N_e}{2\pi r_1^2} [\, B(s, 4.5 - 2s) + C_2\, B(s + d,\, 4.5 - d - 2s)]^{-1} , \tag{20.12}$$

where $B(m, n)$ is the beta function. The values of the parameters depend on shower size ($N_e$), depth in the atmosphere, identity of the primary nucleus, etc. For showers with $N_e \approx 10^6$ at sea level, Greisen uses $s = 1.25$, $d = 1$, and $C_2 = 0.088$. Finally, $x$ is $r/r_1$, where $r_1$ is the Molière radius, which depends on the density of the atmosphere and hence on the altitude at which showers are detected. At sea level $r_1 \approx 78$ m. It increases with altitude.

The lateral spread of a shower is determined largely by Coulomb scattering of the many low-energy electrons and is characterized by the Moliere radius. The lateral spread of the muons ($\rho_\mu$) is larger and depends on the transverse momenta of the muons at production as well as multiple scattering.

There are large fluctuations in development from shower to shower, even for showers of the same energy and primary mass—especially for small showers, which are usually well past maximum development when observed at the ground. Thus the shower size $N_e$ and primary energy $E_0$ are only related in an average sense, and even this relation depends on depth in the atmosphere. One estimate of the relation is [35]

$$E_0 \sim 3.9 \times 10^6 \text{ GeV } (N_e/10^6)^{0.9} \tag{20.13}$$

for vertical showers with $10^{14} < E < 10^{17}$ eV at 920 g cm$^{-2}$ (965 m above sea level). Because of fluctuations, $N_e$ as a function of $E_0$ is not the inverse of Eq. (20.13). As $E_0$ increases the shower maximum (on average) moves down into the atmosphere and the relation between $N_e$ and $E_0$ changes. At the maximum of shower development, there are approximately 2/3 particles per GeV of primary energy.

Detailed simulations and cross-calibrations between different types of detectors are necessary to establish the primary energy spectrum from air-shower experiments [35,36]. Figure 20.7 shows the "all-particle" spectrum. In establishing this spectrum, efforts have been made to minimize the dependence of the analysis on the primary composition. In the energy range above $10^{17}$ eV, the Fly's Eye technique [48] is particularly useful because it can establish the primary energy in a model-independent way by observing most of the longitudinal development of each shower, from which $E_0$ is obtained by integrating the energy deposition in the atmosphere.

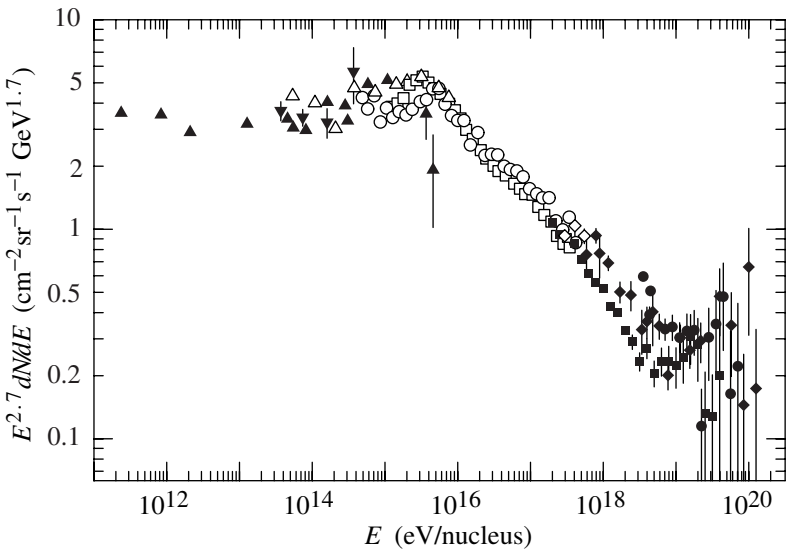


**Figure 20.7:** The all-particle spectrum: ▲ [37], ▼ [38], △ [39], □ [40], ○ [35], ■ [48], ● [42], ♦ [43].

In Fig. 20.7 the differential energy spectrum has been multiplied by $E^{2.7}$ in order to display the features of the steep spectrum that are otherwise difficult to discern. The steepening that occurs between $10^{15}$ and $10^{16}$ eV is known as the *knee* of the spectrum. The feature between $10^{18}$ and $10^{19}$ eV is called the *ankle* of the spectrum. Both these features are the subject of intense interest at present [44].

The *ankle* has the classical characteristic shape [45] of a higher energy population of particles overtaking a lower energy population. A possible interpretation is that the higher energy population represents cosmic rays of extragalactic origin. If this is the case and if the cosmic rays are cosmological in origin, then there should be a cutoff

around $5 \times 10^{19}$ eV, resulting from interactions with the microwave background [46,47]. It is therefore of special interest that several events have been assigned energies above $10^{20}$ eV [48,49,50].

If the cosmic ray spectrum below $10^{18}$ eV is of galactic origin, the *knee* could reflect the fact that some (but not all) cosmic accelerators have reached their maximum energy. Some types of expanding supernova remnants, for example, are estimated not to be able to accelerate particles above energies in the range of $10^{15}$ eV total energy per particle. Effects of propagation and confinement in the galaxy [51] also need to be considered.

**References:**


1. J.A. Simpson, Ann. Rev. Nucl. & Particle Sci. **33**, 323 (1983).
2. Dietrich Müller & Kwok-Kwong Tang, Astrophys. J. **312**, 183 (1987).
3. J.J. Engelmann *et al.*, Astron. & Astrophys. **233**, 96 (1990);
   See also *Cosmic Abundances of Matter* (ed. C. Jake Waddington) A.I.P. Conf. Proceedings No. 183 (1988) p. 111.
4. W.R. Webber, R.L. Golden and S.A. Stephens, in Proc. 20th Int. Cosmic Ray Conf. (Moscow) **1**, 325 (1987).
5. Several new experimental results on antiprotons and positrons were reported and published in the Proceedings of the 24th (Rome) **3** (1995). The positron results are: G. Basini *et al.*, p. 1, J.M. Clem *et al.*, p. 5, F. Aversa *et al.*, p. 9 and G. Tarlé *et al.*, p. 17 (See also S.W. Barwick *et al.*, Phys. Rev. Lett. **75**, 3909 (1995)). The antiproton results are: M. Hof *et al.*, p. 60, A.W. Labrador *et al.*, p. 64, J.W. Mitchell *et al.*, p. 72 and S. Orito *et al.*, p. 76.
6. D.H. Perkins, Astropart. Phys. **2**, 249 (1994).
7. R. Bellotti *et al.*, Phys. Rev. **D53**, 35 (1996).
8. T.K. Gaisser, *Cosmic Rays and Particle Physics*, Cambridge University Press (1990).
9. M.P. De Pascale *et al.*, J. Geophys. Res. **98**, 3501 (1993).
10. K. Allkofer & P.K.F. Grieder, *Cosmic Rays on Earth*, Fachinformationszentrum, Karlsruhe (1984).
11. S. Hayakawa, *Cosmic Ray Physics*, Wiley, Interscience, New York (1969).
12. O.C. Allkofer, K. Carstensen and W.D. Dau, Phys. Lett. **B36**, 425 (1971).
13. B.C. Rastin, J. Phys. **G10**, 1609 (1984).
14. C.A. Ayre *et al.*, J. Phys. **G1**, 584 (1975).
15. I.P. Ivanenko *et al.*, Proc. 19th Int. Cosmic Ray Conf. (La Jolla) **8**, 210 (1985).
16. H. Jokisch *et al.*, Phys. Rev. **D19**, 1368 (1979).
17. F. Halzen, R. Vázquez and E. Zas, Astropart. Phys. **1**, 297 (1993).
18. R.R. Daniel and S.A. Stephens, Revs. Geophysics & Space Sci. **12**, 233 (1974).
19. K.P. Beuermann and G. Wibberenz, Can. J. Phys. **46**, S1034 (1968).
20. I.S. Diggory *et al.*, J. Phys. **A7**, 741 (1974).

21. Paolo Lipari & Todor Stanev, Phys. Rev. **D44**, 3543 (1991).
22. K.S. Hirata *et al.*, (Kam-II Collaboration), Phys. Lett. **B280**, 146 (1992);
    Y. Fukuda *et al.*, Phys. Lett. **B335**, 237 (1994).
23. R. Becker-Szendy *et al.*, (IMB Collaboration), Phys. Rev. **D46**, 3720 (1992);
    See also D. Casper *et al.*, Phys. Rev. Lett. **66**, 2561 (1991).
24. F. Reines *et al.*, Phys. Rev. Lett. **15**, 429 (1965).
25. M.M. Boliev *et al.*, in Proceedings 3rd Int. Workshop on Neutrino Telescopes (ed. Milla Baldo Ceolin), 235 (1991).
26. D. Michael *et al.*, (MACRO) Nucl. Phys. **B35**, 235 (1994) (TAUP-93).
27. R. Becker-Szendy *et al.*, Phys. Rev. Lett. **69**, 1010 (1992);
    Proc. 25th Int. Conf. High-Energy Physics (Singapore, ed. K.K. Phua & Y. Yamaguchi, World Scientific, 1991) p. 662.
28. M. Mori *et al.*, Phys. Lett. **B210**, 89 (1991).
29. M. Crouch, in Proc. 20th Int. Cosmic Ray Conf. (Moscow) **6**, 165 (1987).
30. Yu.M. Andreev, V.I. Gurentzov and I.M. Kogai, in Proc. 20th Int. Cosmic Ray Conf. (Moscow) **6**, 200 (1987).
31. M. Aglietta *et al.*, (LVD Collaboration), Astropart. Phys. **3**, 311 (1995).
32. M. Ambrosio *et al.*, (MACRO Collaboration), Phys. Rev. **D52**, 3793 (1995).
33. Ch. Berger *et al.*, (Frejus Collaboration), Phys. Rev. **D40**, 2163 (1989).
34. K. Greisen, Ann. Rev. Nucl. Sci. **10**, 63 (1960).
35. M. Nagano *et al.*, J. Phys. **G10**, 1295 (1984).
36. M. Teshima *et al.*, J. Phys. **G12**, 1097 (1986).
37. N.L. Grigorov *et al.*, Yad. Fiz. **11**, 1058 (1970) and Proc. 12th Int. Cosmic Ray Conf. (Hobart) **2**, 206 (1971).
38. K. Asakimori *et al.*, Proc. 23rd Int. Cosmic Ray Conf. (Calgary) **2**, 25 (1993);
    Proc. 22nd Int. Cosmic Ray Conf. (Dublin) **2**, 57 and 97 (1991).
39. T.V. Danilova *et al.*, Proc. 15th Int. Cosmic Ray Conf. (Plovdiv) **8**, 129 (1977).
40. Yu. A. Fomin *et al.*, Proc. 22nd Int. Cosmic Ray Conf. (Dublin) **2**, 85 (1991).
41. D.J. Bird *et al.*, Astrophys. J. **424**, 491 (1994).
42. S. Yoshida *et al.*, Astropart. Phys. **3**, 105 (1995).
43. M.A. Lawrence, R.J.O. Reid and A.A. Watson, J. Phys. **G17**, 773 (1991).
44. The most recent discussion is contained in Proc. 24th Int. Cosmic Ray Conf. (Rome) **2**, (1995) as well as the rapporteur talk of S. Petrera at the same conference (to be published). Some important information and discussion can also be found in Ref. 50 (World Scientific, Singapore, to be published).
45. B. Peters, Nuovo Cimento **22**, 800 (1961).
46. K. Greisen, Phys. Rev. Lett. **16**, 748 (1966).

47. G.T. Zatsepin and V.A. Kuz'min, Sov. Phys. JETP Lett. **4**, 78 (1966).

48. D.J. Bird *et al.*, Astrophys. J. **441**, 144 (1995).

49. N. Hayashima *et al.*, Phys. Rev. Lett. **73**, 3941 (1994).

50. A.A. Watson, *Proc. of the 1994 Summer Study on Nuclear and Particle Astrophysics and Cosmology for the Next Millenium*, Snowmass CO, 1994, ed. by E.W. Kolb *et al.* (World Scientific, Singapore, to be published, 1996).

51. V.S. Ptustkin *et al.*, Astron. & Astrophys. **268**, 726 (1993).